ELSEVIER

Cold Regions Science and Technology 23 (1995) 109–119

cold regions science and technology

The compaction of polar snow packs

J.M.N.T. Gray *, L.W. Morland

School of Mathematics, University of East Anglia, Norwich NR4 7TJ, UK

Received 19 August 1993; accepted after revision 17 May 1994

Abstract

As snow is deposited at the surface of a pack, compaction takes place in two stages. There is an initial period of settlement where the rate of volume decrease is dominated by thermal processes, reflecting the rapid metamorphism as branched crystals break down. This is followed by further slower densification as pores collapse, which is largely caused by the overburden. The conventional assumption is that of a linearly viscous relation between the rate of decrease of volume and the pressure, with the viscosity depending on the density and temperature. In view of the long time scales associated with the accumulation of polar snow, compared with observed pore collapse times, an alternative view is that the densification takes place instantaneously, which can be described simply by a pressure–density–temperature relation. This, of course, may depend also on the particular snow structure which is determined by the deposit conditions and subsequent metamorphism. Here, we investigate the special, and much simplified, case of a pressure–density law, ignoring temperature influence, to demonstrate that such a law is consistent with the same data used to infer the viscous law. The function relating density to pressure is determined from observed density profiles with depth, assuming that the snow was deposited at a fixed constant density ρ_0, but no restriction on the accumulation variation is necessary. The model is then used to predict the pressure, density and velocity fields for general surface conditions of deposit density and accumulation rate, to show how the density and velocity fields are influenced by surface conditions for this alternative model. The density profiles with depth are confirmed to be independent of time when the deposit density is held constant, and independent of the accumulation rate variation.

1. Introduction

A description of the mechanical and thermal response of a snow pack to surface forcing by pressure and temperature variation, and to accumulation, involves to some degree an irreversible compaction as pores collapse. Recent investigations of pressure and thermal forcing over seasonal time scales of a dry snow pack comprising firstly ice grains and air (Gray and Morland, 1994), then ice grains, water vapour and air (Gray et al., 1994) made the simplifying assumption of a stationary ice matrix, no compaction, relevant to a fully consolidated pack. This is not satisfactory though during the evolution of a pack due to continuing accumulation.

As snow is first deposited at low density there is a rapid metamorphism as branched crystals break down, for which Anderson (1976) proposes a law relating the rate of volume decrease to temperature. This was subsequently adopted by Jordan (1991) to describe the near surface settlement of recently deposited snow. It is then observed that the deeper snow densifies at a slower rate largely determined by the overburden pressure. Sorge (1935, 1938) concluded from observations of density profiles made in Greenland that the density profile relative to the (rising) snow surface was approximately independent of time. Bader (1954) drew attention to these observations and proposed a

* Corresponding author.

SSDI 0165-232X(94)00010-U

linearly viscous law (Bader, 1960, 1962), between snow pressure, p, and the vertical strain-rate, $\dot{\epsilon}_z$, with a density dependent compactive viscosity, η_c, to describe the process. Using the snow mass balance 2.8 (derived later) this relationship can be expressed as

$$\frac{p}{\eta_c} = \frac{1}{\rho}\frac{\mathrm{d}\rho}{\mathrm{d}t} \equiv -\dot{\epsilon}_z \tag{1.1}$$

for snow density ρ. In the steady-state when the density profile with depth is time-invariant and the accumulation rate is held constant (no intervals between snow falls), the compactive viscosity can then be determined. Based on these assumptions Kojima (1964) drew together an extensive set of Antarctic depth–density profiles extending to 10 m, from which he deduced the form of the compactive viscosity as a function of density. Yoshida et al. (1956) proposed a further dependence on the absolute temperature of the snow. This has been adopted in some current numerical models (e.g. Bader and Weilenmann, 1992; Jordan, 1991).

Mellor (1975) expressed some reservations to this approach. He suggested that when new snow falls, each underlying layer densifies rapidly, but when accumulation stops the compaction becomes insignificant. That is, the densification occurs in events of limited duration, rather than as steady creep. The apparent value of a compactive viscosity correlation must then hinge on the interval between snow falls, and is not strictly a material property. He further concluded that constitutive properties of snow exhibited such bewildering complexities that it was necessary to adopt greatly simplified descriptions, concentrating on the characteristics that dominate in a particular problem. We now take this alternative view that the densification takes place on much shorter time scales than the accumulation and so is described by an instantaneous response relating pressure to density and temperature. We make the further simplification here that pressure depends only on density, ignoring temperature. The process is assumed irreversible, so there would be no density decrease due to removal of the pressure. This model, therefore, predicts that each snow layer moves vertically downwards as it compacts during accumulation, but when there is no accumulation the motion ceases. In reality we would expect further creep under the overburden stress, but this would eventually decay without increase of the overburden. That is, the response would better be described by a viscoelastic law. A viscous law is the other extreme, which predicts indefinite creep under a constant overburden.

To determine the function relating density to pressure directly from given density profiles with depth, it is necessary to assume that the snow was deposited at a fixed density ρ_0 during the whole evolution of the pack, but no restriction on the accumulation variation is necessary. However, correlating a viscous model with a density profile requires the further assumption of a constant surface accumulation rate, with no intervals between snow falls during the entire pack development. We use the same density profile data here to construct our pressure–density relation as Kojima (1964) used to determine the dependence of the compactive viscosity on density. This supposes that there is a universal pressure–density law for all snow structures, independent of any thermal processes which take place. The model is then used to determine the pressure, density and velocity fields for general surface conditions of deposit density and accumulation rate, to show how the density and velocity fields are influenced by surface conditions.

2. Pack evolution equations

The dry snow pack is viewed as an interacting mixture of rigid ice grains and air occupying the pore space in the matrix. The three-dimensional mass, momentum and energy balances for this two constituent model have been formulated in the framework of interacting continua theory by Gray and Morland (1994). These equations are used as a starting point for our analysis and we focus on a one-dimensional vertical snow pack that has no lateral gradients and whose horizontal velocity components are identically zero.

In each element of the snow pack there is a proportion of each of the constituents, defined by the volume fraction of constituent ν per unit volume of mixture, ϕ^ν. Adopting the same notation as Gray and Morland (1994), the constituent letters $\nu = \mathrm{a,i}$ are used to refer to the air and ice respectively. By definition the volume fractions lie between zero and unity, with unit sum:

$$0 \le \phi^\nu \le 1, \quad \phi^{\mathrm{a}} + \phi^{\mathrm{i}} = 1 \tag{2.1}$$

Partial variables are defined per unit mixture volume, while intrinsic variables are defined per unit constituent

volume. The partial density and pressure are related to their intrinsic counterparts by linear volume fraction scalings

$$\rho^{\nu}=\phi^{\nu}\rho^{N}, \quad p^{\nu}=\phi^{\nu}p^{N} \tag{2.2}$$

where the superscript constituent letters are lower case for partial and upper case for intrinsic variables. A detailed three-dimensional formulation of mixture theory with such interpretations is presented by Morland (1992). The mixture density ρ and mixture pressure p are given by summing the partial density and partial pressure over each constituent, respectively

$$\rho^{a}+\rho^{i}=\rho, \quad p^{a}+p^{i}=p \tag{2.3}$$

Both constituents satisfy a mass balance equation of the form

$$\frac{\partial \rho^{\nu}}{\partial t}+\frac{\partial}{\partial z}(\rho^{\nu}v^{\nu})=0 \quad (\nu=\mathrm{i,a}) \tag{2.4}$$

where z denotes the vertical co-ordinate measured in the upward sense, and v^{ν} is the vertical velocity component of constituent ν. For the very slow motions arising in a snow pack the momentum conservation equations reduce to the equilibrium equations

$$-\frac{\partial p^{\nu}}{\partial z}-\rho^{\nu}g+\rho B^{\nu}=0 \tag{2.5}$$

where g is the gravitational body force, and ρB^{ν} is the interaction drag exerted on constituent ν by the other constituents per unit volume of mixture.

By definition the interaction drag experienced by the ice due to the motion of the gas, ρB^{i}, is equal in magnitude but opposite in sign to the interaction drag experienced by the gas, ρB^{a}, as it passes through the ice matrix. Thus, the interaction drag can be eliminated by summing the air and ice momentum balances (2.5), and, using (2.3), a simple relation between the mixture density and mixture pressure is obtained:

$$\frac{\partial p}{\partial z}=-\rho g \tag{2.6}$$

The sum of the air and ice mass balances (2.4) can be expressed in the form

$$\frac{\partial \rho}{\partial t}+\frac{\partial}{\partial z}(\rho v^{i})+\frac{\partial}{\partial z}[\rho^{a}(v^{a}-v^{i})]=0 \tag{2.7}$$

Using (2.2) and (2.3) the snow density is given by $\rho=\phi^{i}\rho^{I}+\phi^{a}\rho^{A}$, which implies that $\rho^{a} \ll \rho$ for intrinsic densities $\rho^{I}=918$ kg m^{-3}, $\rho^{A}\simeq 1$ kg m^{-3}, and typical volume fractions of comparable magnitude. The upward air velocity v^{a} resulting from the loss of pore space as the matrix collapses, maximum if there is free drainage, should not exceed $|v^{i}|$ by too great a factor, so $|\rho^{a}v^{a}| \ll |\rho v^{i}|$ is assumed. Then the total snow mass balance equation (2.7) is approximated by

$$\frac{\partial \rho}{\partial t}+\frac{\partial}{\partial z}(\rho v^{i})=0 \tag{2.8}$$

The conservation equations (2.6), (2.8) need a constitutive relation for the pack pressure, which will describe the irreversible collapse of the pore space, to close the system. As described in the introduction, we now propose to investigate a constitutive law which simply relates pressure to density. A convenient form is

$$\frac{\rho-\rho_s}{1-\rho_s}=\hat{f}(p-p^{A}), \quad \hat{f}(0)=0 \tag{2.9}$$

where the function $\hat{f}$ is to be determined from field observations, and the reference density ρ_s is the density at which the snow element was deposited at the pack's surface where the pressure was the constant atmospheric pressure p^{A}. The reference density is therefore a constant for each ice particle and must be conserved along its particle path, thus

$$\frac{\partial \rho_s}{\partial t}+v^{i}\frac{\partial \rho_s}{\partial z}=0 \tag{2.10}$$

We shall suppose that at $t=0$ the snow starts to accumulate on a fixed impervious horizontal surface, at $z=0$. At the lower boundary we therefore apply the condition that the ice velocity $v^{i}\equiv 0$. For a normal accumulation flux $q(t)$ per unit mixture area per unit time, the kinematic condition which describes the evolution of the snow surface, $z=h(t)$, is

$$\dot{h}(t)=v^{i}(h,t)+q(t) \tag{2.11}$$

where the dot indicates differentiation with respect to time. The evolution of the free surface is therefore dependent on the internal deformation of the pack through $v(h,t)$ during the collapse, as well as on the snow accumulation rate. At $z=h$ the total pressure p is at atmospheric pressure p^{A} and the surface density

defines the reference density ρ_s of the current surface element. Thus, we must solve Eqs. (2.6), (2.8), (2.9) and (2.10) subject to the initial conditions

$$t=0,\ z=0:\ v^{\mathrm{i}}=0,\ p=p^{\mathrm{A}},\ \rho=\rho_s=\rho_h(0) \tag{2.12}$$

and the boundary conditions

$$\left.\begin{array}{l} z=0:\ v^{\mathrm{i}}=0 \\ z=h:\ \dot{h}(t)=v^{\mathrm{i}}(h,t)+q(t),\ p=p^{\mathrm{A}}, \\ \qquad \rho(h,t)=\rho_s(h,t)=\rho_h(t) \end{array}\right\} \tag{2.13}$$

where $\rho_h=\rho_h(t)$ is the density at which the snow falls at the surface. Despite the apparent simplicity of the equations this problem involves a moving interface at which boundary conditions must be applied, and the interface position is itself part of the solution. Numerical methods to treat *moving boundary value problems* are not routine. A fixed domain mapping technique (Morland, 1982) is adopted for our solution construction and applications.

The dominant forcing arises from the snow deposited at the surface, which is the cause of the densification process. Typical accumulation rates are of order $q^* \simeq 1$ m yr^{-1} and ice matrix velocities can approach this value in the near surface layers, suggesting the velocity scaling magnitude $v^*=(z^*/t^*)=q^*$. For the forcing scenarios envisaged it is appropriate to use a time scale $t^*=1$ year and length scale $z^*=1$ metre. It is sensible to scale the snow density, ρ, the reference density, ρ_s, and the surface density, ρ_{h}, on the intrinsic ice density ρ^{I} which is their maximum attainable magnitude. Finally, the boundary condition (2.13) implies that the pressure at the free surface is always at atmospheric pressure, and the hydrostatic balance in (2.6) suggests a perturbation from atmospheric pressure with depth as the overburden of snow increases. Thus, we introduce non-dimensional variables

$$t=t^*\tilde{t},\ z=z^*\tilde{z},\ v^{\mathrm{i}}=v^*\tilde{v},\ q=q^*\tilde{q},\ \rho=\rho^{\mathrm{I}}\tilde{\rho},$$
$$\rho_s=\rho^{\mathrm{I}}\tilde{\rho}_s,\ \rho_h=\rho^{\mathrm{I}}\tilde{\rho}_h,\ p=p^{\mathrm{A}}+\rho^{\mathrm{I}}gz^*\tilde{p} \tag{2.14}$$

where

$$q^*=v^*=3\times10^{-8}\ \mathrm{m\ s^{-1}},$$
$$t^*=3\times10^{7}\ \mathrm{s},\ z^*=1\ \mathrm{m} \tag{2.15}$$

and the tilde denotes a non-dimensional variable. The non-dimensional equations are

$$\frac{\partial\tilde{\rho}}{\partial\tilde{t}}+\frac{\partial}{\partial\tilde{z}}(\tilde{\rho}\tilde{v})=0 \tag{2.16}$$

$$\frac{\partial\tilde{\rho}_s}{\partial\tilde{t}}+\tilde{v}\frac{\partial\tilde{\rho}_s}{\partial\tilde{z}}=0 \tag{2.17}$$

$$\frac{\partial\tilde{p}}{\partial\tilde{z}}=-\tilde{\rho} \tag{2.18}$$

$$\frac{\tilde{\rho}-\tilde{\rho}_s}{1-\tilde{\rho}_s}=f(\tilde{p}) \tag{2.19}$$

where $f(\tilde{p})=\hat{f}(p\text{-}p^A)$. These equations are subject to the initial conditions

$$\tilde{t}=0,\ \tilde{z}=0:\ \tilde{v}=0,\ \tilde{p}=0,\ \tilde{\rho}=\tilde{\rho}_s=\tilde{\rho}_h(0), \tag{2.20}$$

and the boundary conditions

$$\left.\begin{array}{l} \tilde{z}=0:\ \tilde{v}=0 \\ \tilde{z}=\tilde{h}:\ \dot{\tilde{h}}(\tilde{t})=\tilde{v}(\tilde{h},\tilde{t})+\tilde{q}(\tilde{t}),\ \tilde{p}=0, \\ \qquad \tilde{\rho}(\tilde{h},\tilde{t})=\tilde{\rho}_s(\tilde{h},\tilde{t})=\tilde{\rho}_h(\tilde{t}) \end{array}\right\} \tag{2.21}$$

This notation is cumbersome so we shall omit the tildes on the implicit understanding that non-dimensional variables are used henceforth throughout the remainder of the text.

3. Construction of pressure density law

Eq. (2.17) indicates that ρ_s equals ρ_h evaluated at the time of its deposition along a given particle path. In the special case that ρ_h is constant and equal to ρ_0 (say) over the whole accumulation history, then ρ_s will be equal to ρ_0 along every particle path, and, therefore, the reference density $\rho_s\equiv\rho_0$ throughout the pack. In this situation (2.18) and (2.19) are equations for p and ρ independent of the velocity field v. We now show how, with the further assumption that ρ and p are functions of depth

$$s=h(t)-z \tag{3.1}$$

with no other dependence on t, and with the profile $\rho=\rho(s)$ given by data, (2.18) and (2.19) determine the function $f(p)$. By (2.18) and the surface condition $(2.21)_2$,

$$p(s)=\int_0^s\rho(s')\mathrm{d}s' \tag{3.2}$$

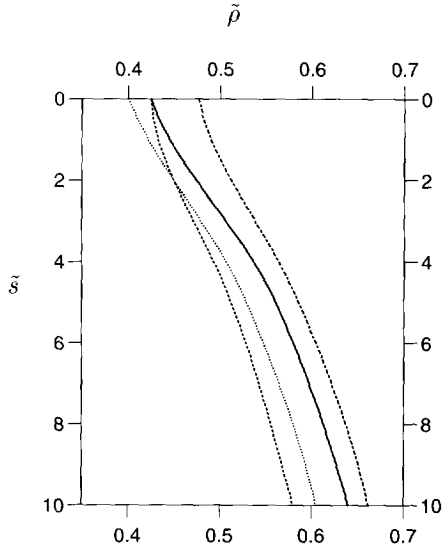

Fig. 1. The non-dimensional density profile with depth at sites EH 60 #29 (bold line), NV 59 II (dashed line), EH 60 #8 (dotted line) and BH 58 III (dot-dashed line). These curves are derived from the experimental data of Kojima (1964).

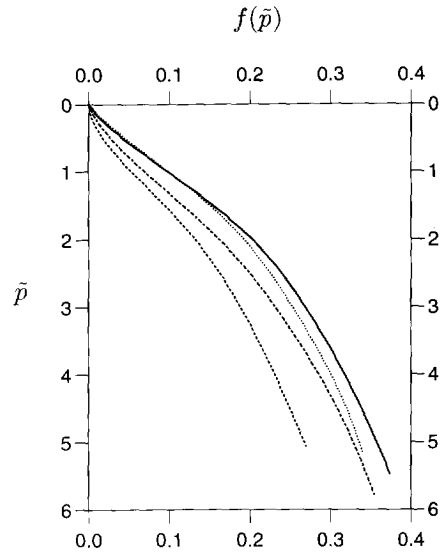

Fig. 2. The pressure–density relation, $f(\tilde{p})$, corresponding to sites EH 60 #29 (bold line), NV 59 II (dashed line), EH 60 #8 (dotted line) and BH 58 III (dot-dashed line). These curves are derived from the experimental data of Kojima (1964).

and by (2.19) with $\rho_s \equiv \rho_0$,

$$f[p(s)] = \frac{\rho(s) - \rho_0}{1 - \rho_0} \tag{3.3}$$

and $\rho(s), p(s)$ and $f[p(s)]$ are strictly increasing functions of s. Therefore, plotting $p(s)$ against $f[p(s)]$ for the given $\rho(s)$ determines $f = f(p)$. It should be emphasized that this correlation is entirely independent of the accumulation rate variation during the pack evolution, in contrast to the correlation with a viscous law (Kojima, 1964) which applies only if the accumulation rate remains constant throughout. The present model therefore allows consistent applications to varying surface accumulation, which is not necessarily the case with the viscous law. The model function $f(p)$, however, could also be site dependent, depending on the deposited snow structure.

The observed density variations at four sites in Antarctica known as NV 59 II, EH 60 #8, EH 60 #29 and BH 58 III (Kojima, 1964) are illustrated in Fig. 1 in non-dimensional density and spatial units. Each of the curves have a similar shape with density increasing monotonically with depth, and the largest density gradients occur between 1 and 5 spatial units. Following the procedure described in Eqs. (3.2), (3.3), the pressure and $f(p)$ are computed at regular spatial intervals at each site. Then $f(p)$ is plotted as a function of p as illustrated in Fig. 2. Three of the curves lie in quite a narrow region of the graph, which suggests that an approximately common function f might be found. The data from site EH 60 #29 was used to model the function f in the investigations presented here. An accurate Chebyshev polynomial representation of $f(p)$ was constructed for inclusion in the numerical algorithm developed to solve the system for the general surface conditions $(2.21)_2$. This can apply only to the pressure range correlated, and extrapolation to higher pressures would require a different representation. Site NV 59 II appears to be slightly anomalous, this could be due to a variation in the history of surface density accumulation which is discussed at further length in Section 4, or a manifestation of some sort of temperature dependence that is beyond the scope of this paper.

4. Solution for general surface conditions

The one-dimensional model presented in Section 2 is a non-linear system of partial differential equations for p, ρ, ρ_s, v and the surface position $h(t)$, which is complicated by the presence of a moving boundary at

the surface of the snow pack, and hence a solution will only be available by numerical means. For problems involving moving boundaries direct numerical methods are suspect. Here we adopt a fixed domain mapping technique (Morland, 1982), which has been successfully implemented by Kelly et al. (1990) for permafrost evolution. The boundary is now specified and the boundary velocity becomes an unknown variable.

We make a change of variables in which the spatial co-ordinate z remains unchanged, but the snow depth h, strictly increasing with time, is adopted as an independent variable in place of time t. This analysis, therefore, does not extend to the limit $\dot{h}(t)=0$, and so the method fails if there are periods with no snow fall.

The evolution equations (2.16)–(2.19) become, in the (z,h) domain without changing function notation,

$$\gamma\frac{\partial\rho}{\partial h}+\frac{\partial}{\partial z}(\rho v)=0 \tag{4.1}$$

$$\gamma\frac{\partial\rho_s}{\partial h}+v\frac{\partial\rho_s}{\partial z}=0 \tag{4.2}$$

$$\frac{\partial p}{\partial z}=-\rho \tag{4.3}$$

$$\frac{\rho-\rho_s}{1-\rho_s}=f(p) \tag{4.4}$$

where

$$\gamma(h)=\frac{\mathrm{d}h}{\mathrm{d}t} \tag{4.5}$$

is the interface velocity. Once $\gamma(h)$ is determined the time t for any h is given by

$$t=\int_0^h\frac{\mathrm{d}h'}{\gamma(h')} \tag{4.6}$$

These equations are subject to the initial conditions

$$h=0,\ z=0:\ v=0,\ p=0,\ \rho=\rho_s=\rho_h(0) \tag{4.7}$$

and the boundary conditions

$$\left.\begin{aligned} &z=0:\ v(0,h)=0,\\ &z=h:\ \gamma(h)=v(h,h)+q(h),\ p=0,\\ &\qquad\rho(h,h)=\rho_s(h,h)=\rho_h(h)\end{aligned}\right\} \tag{4.8}$$

The snow pack configuration is illustrated in Fig. 3. It occupies the lower triangular region between the h axis,

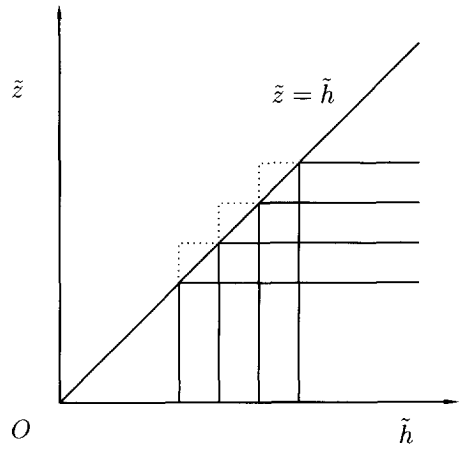

Fig. 3. The (z,h) domain for the snow pack.

which is the fixed impervious boundary $z=0$, and the surface interface position, $z=h$, which lies along the 45° line in (z,h) space. Thus, a regular discretization scheme, with equal uniform steps in z and h, ensures that all the boundary conditions are evaluated at a grid node. Note that a direct method would have to apply the boundary conditions at some estimated position between adjacent grid cells on the upper boundary.

The reduced system of equations is intimately coupled and the numerical algorithm uses an initial estimate at each thickness increment to start an iterative procedure in which the calculated solution is refined until the accuracy meets some prescribed criterion. Taylor series are used to construct a solution to (4.1)–(4.8) valid for small z and h, which is then used to initialise the variables and derivatives that are needed to start the numerical algorithm from the level $3h$.

The iterative procedure is improved by first changing the equation structure. In most forcing scenarios we would expect the variation in the surface density ρ_h to be quite slow, perhaps taking place over a number of years. It is therefore advantageous to eliminate the density $\rho(z,h)$ in favour of the reference density $\rho_s(z,h)$ by (4.4), and express the pressure Equation (4.3) as

$$\frac{\partial p}{\partial z}=-[\rho_s+(1-\rho_s)f(p)] \tag{4.9}$$

Thus, given a good estimate of ρ_s and a representation of $f(p)$ constructed from the observed pit measurements at site EH 60 #29 (Kojima, 1964) described in Section 3, the pressure can be computed using a fourth

order Runge–Kutta scheme. The density is then obtained from the algebraic relation

$$\rho = \rho_s + (1-\rho_s) f(p) \tag{4.10}$$

The surface velocity $v(h,h)$ can then be obtained by integrating (4.1) through the snow depth h and applying the zero velocity condition at $z=0$. Next, using the relation $\gamma(h) = v(h,h) + q(h)$ from (4.8), it follows that

$$\gamma(h) = \rho_h(h) q \left\{ \rho_h(h) - \int_0^h \frac{\partial \rho}{\partial h} \, \mathrm{d}z \right\}^{-1} \tag{4.11}$$

which allows γ to be estimated in terms of externally prescribed functions ρ_h and q, and the density ρ for which we already have an estimate. Finally, the velocity is estimated by

$$v(z,h) = -\frac{\gamma}{\rho} \int_0^z \frac{\partial \rho}{\partial h} \, \mathrm{d}z' \tag{4.12}$$

and the real time t is determined by (4.6). With these fields, (4.2) subject to the surface conditions (4.8) can be numerically integrated to determine a new reference density $\rho_s(z,h)$ to perform the cycle again. Subsequently, at the end of successive cycles, the change in each variable at each z is tested until the maximum difference was less than 10^{-8} in magnitude. The results can then be mapped back into space and time variables (z,t).

5. Illustrations

In all the simulations presented no snow is present initially and the pack is built up over a 12 year period. The depth which the snow reaches after this period, and the evolution of the density structure within the pack, are both dependent on the density ρ_h at which the snow is deposited and the rate of snow accumulation q, which are functions of time. Five basic forcing scenarios are considered here:

$$\begin{aligned}
&\text{(i)} && \rho_h = 0.425, \quad q = 1 \\
&\text{(ii)} && \rho_h = 0.375 + (0.475 - 0.375)\, t/12, \quad q = 1 \\
&\text{(iii)} && \rho_h = 0.475 + (0.375 - 0.475)\, t/12, \quad q = 1 \\
&\text{(iv)} && \rho_h = 0.425, \quad q = 0.5 + (1.5 - 0.5)\, t/12 \\
&\text{(v)} && \rho_h = 0.425, \quad q = 1.5 + (0.5 - 1.5)\, t/12
\end{aligned} \tag{5.1}$$

The simplest is case (i), in which both q and ρ_h are constant during the entire evolution history of the pack. Case (ii) keeps the rate of accumulation constant but changes the surface density from 0.375 to 0.475 linearly in time over a twelve year period, while case (iii) performs the same simulation with the opposite sense to the density variation. Cases (iv) and (v) keep the surface density constant and vary the accumulation rate instead, from 0.5 to 1.5 and from 1.5 to 0.5 respectively, with a linear variation in time over the same 12 year period.

The reduced theory described in Section 3, in which the deposition density ρ_h is held constant, applies in cases (i), (iv) and (v), and the density profiles plotted as a function of depth should, therefore, be time invariant. The solid line plotted in Figs. 4 and 5 shows the density, ρ, as a function of depth, $s = h - z$, for case (i) at time $t=6$ and $t=12$ respectively. Not only do the two curves coincide exactly over the common interval, confirming the time invariance, but they also coincide with the density profile at site EH 60 #29 (Fig. 1) that was used to construct $f(p)$, demonstrating the accuracy of the numerical algorithm. The density profiles for cases (ii) (dashed line) and (iii) (dotted line) are also illustrated in Figs. 4 and 5, and demonstrate that a lower density gradient is indicative of an increase in the deposition density ρ_h, and larger gradients correspond to a reduction in ρ_h. Indeed, the dashed line in Fig. 4 fits very closely to the anomalous density profile at site NV 59 II, mentioned in Section 3, which could, therefore, be explained by an increase in deposition density in the recent past. Note that the density profiles are not very

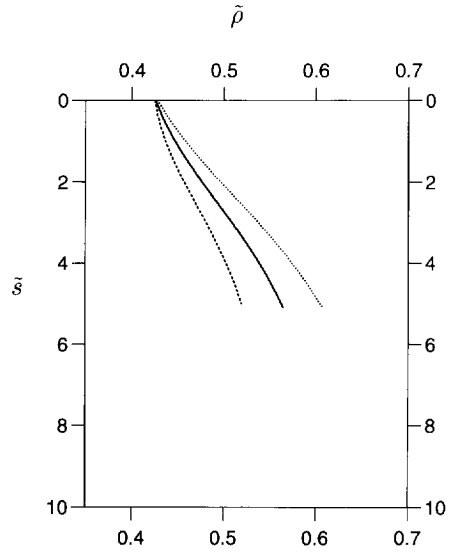

Fig. 4. Non-dimensional density profiles with depth at $\tilde{t}=6$ predicted for cases (i) (bold line), (ii) (dashed line) and (iii) (dotted line).

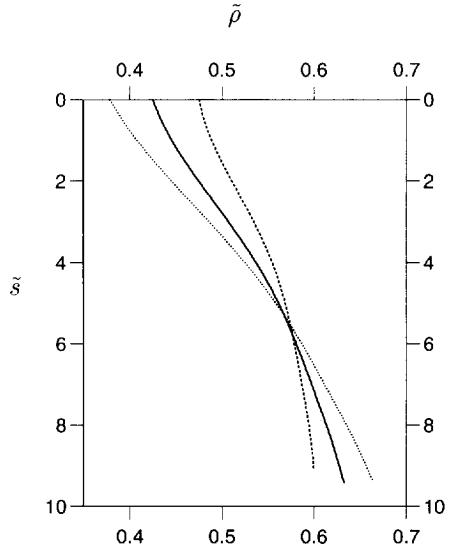

Fig. 5. Non-dimensional density profiles with depth at $\tilde{t}=12$ predicted for cases (i) (bold line), (ii) (dashed line) and (iii) (dotted line).

sensitive to variations in the mean deposition density ρ_h.

Fig. 6 is a contour plot of the density $\rho(z,t)$ for case (i), each contour interval is equally spaced, starting at $\rho=0.425$ at the surface indicated by the dashed line. Each of the contour lines are parallel to the surface, which is also true in cases (iv) and (v) (not illustrated), indicating that the density profile with depth is time invariant. The corresponding velocity contours are shown in Fig. 7. The velocity at any given point is dependent on the local density change and the velocity

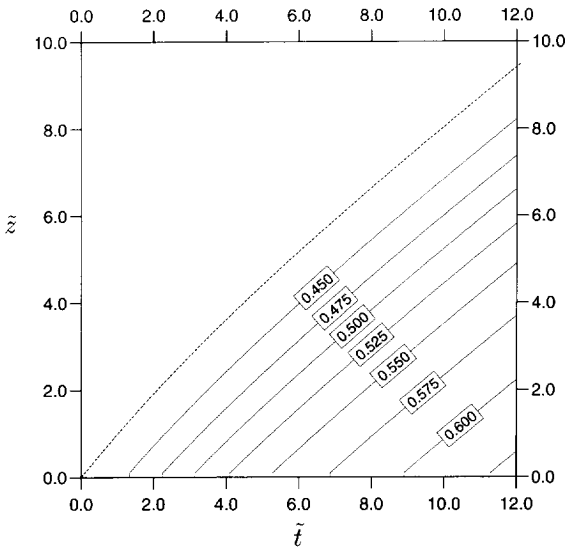

Fig. 6. Contours of density $\tilde{\rho}$ in space–time $(\tilde{z},\tilde{t})$ for case (i). At the dotted line, which defines the snow surface height variation with time above the fixed lower boundary at $z=0$, the density $\tilde{\rho}=0.425$.

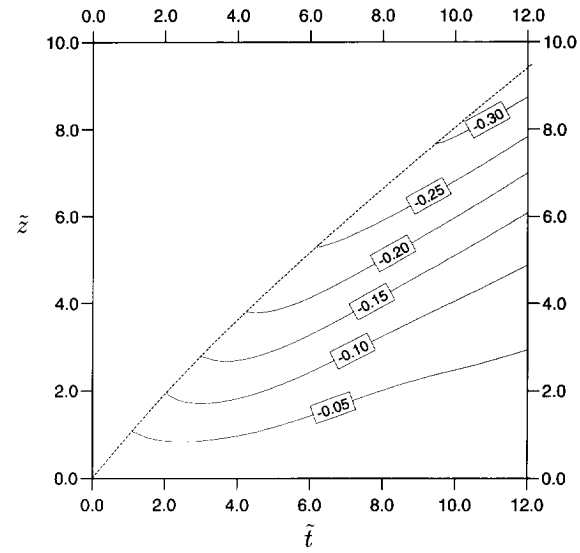

Fig. 7. Contours of velocity $\tilde{v}$ in space–time $(\tilde{z},\tilde{t})$ for case (i). The dotted line defines the snow surface height variation with time above the fixed lower boundary at $z=0$.

of the layer immediately below it. Thus, close to the time axis where the velocity is specified by the basal boundary condition to be identically zero, the velocity magnitudes are small, and the velocity increases monotonically to a maximum at the surface. The deeper the snow pack the larger the surface velocity magnitude becomes, tending to a finite limit as the density in the lower layers approaches the fully compacted ice density. The velocity contours for (ii) and (iii) are both very similar in shape to case (i), but the velocity magnitudes are slightly greater in case (ii) and slightly less in case (iii) reflecting the greater capacity for compaction when denser snow accumulates on top of lighter snow, and vice versa. It follows, necessarily, that the depth of snow is greatest when least compaction occurs within the pack. This is born out by the results; case (iii) has the highest free surface, then case (i) and case (ii) have successively lower free surfaces.

Since the compaction velocities are all approximately the same, the increase in density of any element in the snow pack is also approximately the same in cases (i), (ii) and (iii). This has an important effect on the density distribution. In case (ii) the basal layers of the snow pack are deposited with a reduced density, and therefore for the same level of density increase as case (i) will have a lower density throughout the snow pack evolution. However, the surface layers in case (ii) are deposited with progressively increasing deposit density and will have an enhanced density for the same level of compaction. The density contours in case (ii), illustrated in Fig. 8, lie closer to the vertical than in case (i), indicating that the density gradient with depth has been reduced. This suggests that, for more dramatic changes in the deposit density, layers of higher density may overly less dense layers. A similar argument in case (iii) leads to enhanced densities in the basal layers and lower near surface densities, resulting in much higher density gradients with depth, as illustrated in Fig. 9. The reference density in scenarios (i), (iv) and (v) is of little interest as it remains at the constant value, 0.425. However, in cases (ii) and (iii) the reference density changes from 0.375 to 0.475 and vice versa over the 12 year period. In these cases the reference density acts as a passive tracer whose contours, illustrated for case (iii) in Fig. 10, trace out the particle paths as compaction occurs.

Although variation of the accumulation rate q does not have any effect on the density profile, it does have a profound effect on the position of the free surface and the velocity distribution within the pack. The velocity contours for cases (iv) and (v) are illustrated in Figs. 11 and 12 respectively. In case (iv) the deposition

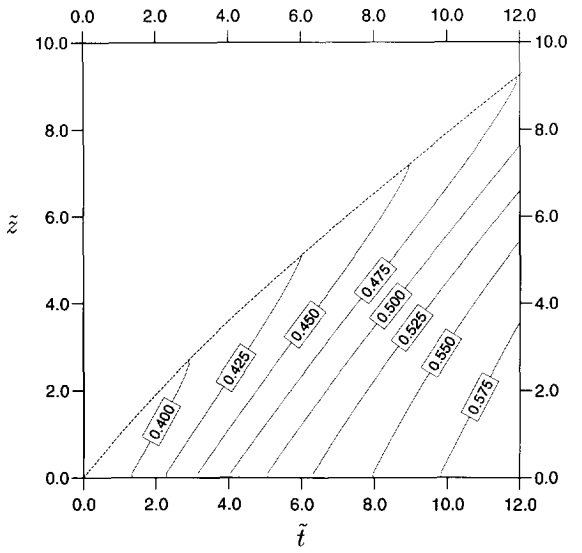

Fig. 8. Contours of density $\tilde{\rho}$ in space–time $(\tilde{z},\tilde{t})$ for case (ii). The dotted line defines the snow surface height variation with time above the fixed lower boundary at $z=0$.

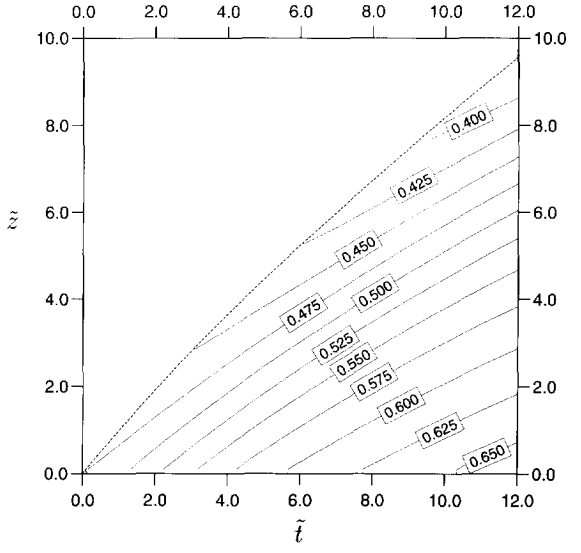

Fig. 9. Contours of density $\tilde{\rho}$ in space–time $(\tilde{z},\tilde{t})$ for case (iii). The dotted line defines the snow surface height variation with time above the fixed lower boundary at $z=0$.

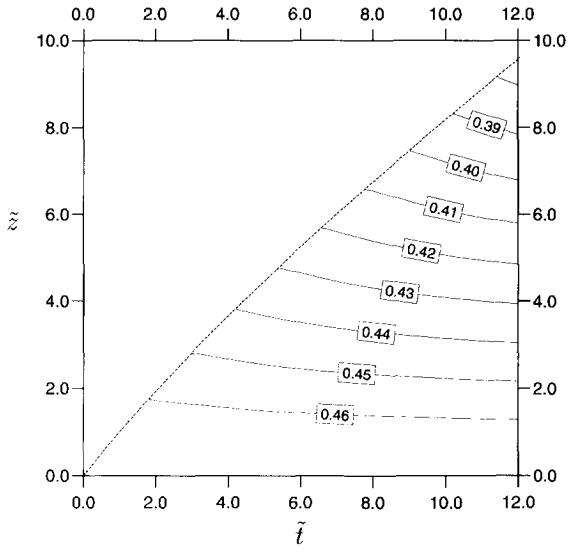

Fig. 10. Contours of reference density $\tilde{\rho}_s$ in space–time $(\tilde{z},\tilde{t})$ for case (iii). The dotted line defines the snow surface height variation with time above the fixed lower boundary at $z=0$.

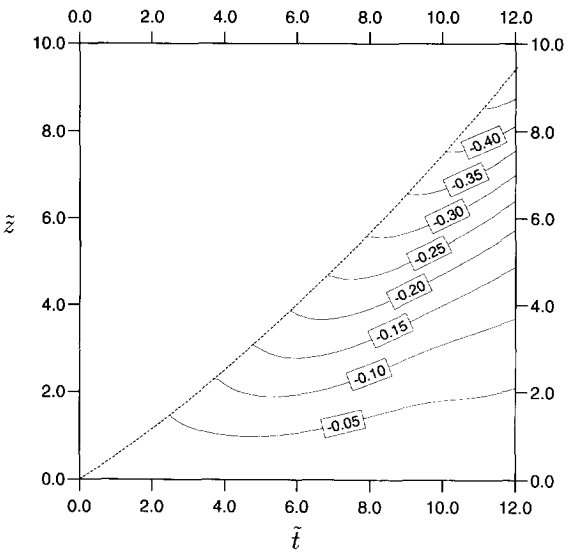

Fig. 11. Contours of velocity $\tilde{v}$ in space–time $(\tilde{z},\tilde{t})$ for case (iv). The dotted line defines the snow surface height variation with time above the fixed lower boundary at $z=0$.

starts off slowly so that initially the depth of snow that has been built up is less than in case (i) at the same instant of time, and the interface velocity γ and the internal deformation velocities are also reduced. Above $t=6$, the snow accumulates faster than in case (i) and

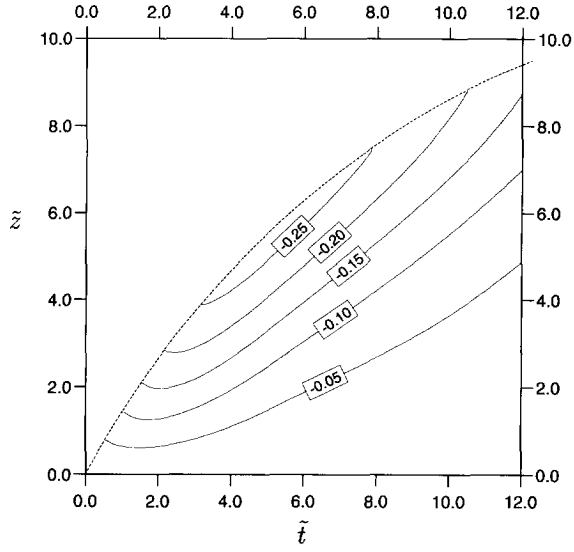

Fig. 12. Contours of velocity $\tilde{v}$ in space–time $(\tilde{z},\tilde{t})$ for case (v). The dotted line defines the snow surface height variation with time above the fixed lower boundary at $z=0$.

the velocities are correspondingly increased. This gives the free surface a concave shape plotted against time as shown in Fig. 11. In case (v) the opposite is true; compaction velocities are enhanced up to $t=6$ and are then reduced in the later stages as the amount of accumulation decreases, and a the graph of the free surface position with time is convex. In all five scenarios the pressure is hydrostatic, increasing with depth from the $p=0$ boundary condition applied at the free surface.

6. Summary

A simple pressure–density constitutive relation has been investigated which provides an alternative approach, to the conventional linearly viscous relation, and has a number of features to recommend it. Correlating observed steady-state depth–density profiles to a viscous law (Kojima, 1964), to infer a compactive viscosity, requires that both the snow deposit density and the accumulation rate are constant throughout the entire development of the pack. Thus, the apparent value of the compactive viscosity at a particular site hinges on the interval between snow falls, which is not strictly a material property. However, correlation of the pressure–density function is entirely independent of the

accumulation rate history and therefore allows consistent applications to varying surface accumulation, which is not necessarily the case with the viscous law. The function $f(p)$, which determines the response of the pressure–density law, may be site specific as it is independent of any thermal processes which take place. More complicated dependencies that take account of the temperature and the snow structure may allow a universal pressure–density function to be determined in future, but is beyond the scope of this paper.

With the proposed model each underlying layer densifies instantaneously as new snow falls, but when there is no accumulation the motion ceases; that is, the delayed creep present with a viscous law does not occur. This reflects layer profile observations (Mellor, 1975) in which snow densifies rapidly during accumulation and vertical creep decays to a relatively insignificant rate after the snow fall. If the accumulation deposit density is constant the constitutive relation yields Sorge's law (1935; 1938) completely independently of the accumulation rate. In this situation, therefore, the depth–density profile will be exactly the same whether the accumulation is uniform in time or takes place in a completely general manner, with intervals between snow falls. Variations in the deposit density are remembered throughout the life time of the pack, and the associated depth–density profiles are much more complicated.

Acknowledgements

This work has been supported by the Natural Environment Research Council.

References

Anderson, E.A., 1976. A point energy and mass balance model of a snow cover. Office of Hydrology, National Weather Service, Silver Spring, Maryland, NOAA Technical Report NWS 19.

Bader, H., 1954. Sorge's law of densification of snow on high polar glaciers. J. Glaciol., 2(15): 319–323.

Bader, H., 1960. Theory of densification of dry snow on high polar glaciers, I. CRREL Research Report 69.

Bader, H., 1962. Theory of densification of dry snow on high polar glaciers, II. CRREL Research Report 108.

Bader, H.P. and Weilenmann, P., 1992. Modeling temperature distribution, energy and mass flow in a (phase-changing) snowpack. I. Model and case studies. Cold Reg. Sci. Technol., 20: 157–181.

Gray, J.M.N.T. and Morland, L.W., 1994. A dry snow pack model. Cold Reg. Sci. Technol., 22(2): 135–148.

Gray, J.M.N.T., Morland, L.W. and Morris, E.M., 1994. A phase changing dry snow pack model. J. Glaciol., in press.

Jordan, R. 1991. A one-dimensional temperature model for a snow cover: technical documentation for SNTHERM.89. CRREL Special Report, 91-16, pp. 1–49.

Kelly, R.J., Morland, L.W. and Boulton, G.S., 1990. Deep penetration of permafrost through saturated ground. Cold Reg. Sci. Technol., 18: 9–27.

Kojima, K., 1964. Densification of snow in Antarctica. In: M. Mellor (Editor), Antarctic Snow and Ice Studies Antarctic Research Series, 2. American Geophysical Union.

Mellor, M., 1975. A review of basic snow mechanics. In: Snow Mechanics Symposium (Proceedings of the Grindelwald Symposium, April 1974). IAHS–AISH, 114: 251–291.

Morland, L.W., 1982. A fixed domain method for diffusion with a moving boundary. J. Eng. Math., 16: 259–269.

Morland, L.W., 1992. Flow of viscous fluids through a porous deformable matrix. Surv. Geophys., 13: 209–268.

Sorge, E., 1935. Glaziologische Untersuchungen in Eismitte. In: Wissenschaftliche der Deutschen Groenland-Expedition Alfred Wegner, 3. Brockhaus, Leipzig, p. 270.

Sorge, E., 1938. Die Firnschrumpfung in der obersten Schichten des Groenlaendischen Inlandeises. International Geodetic and Geophysical Union. Association of Scientific Hydrology, Vol. 23, pp. 725–731.

Yoshida, Z. et al., 1956. Physical studies on deposited snow. Contributions from the Institute of Low Temperature Science, No. 9. Hokkaido University.